DIRECT NUMERICAL SIMULATION OF THE FLOW AROUND AN ARRAY OF CYLINDERS

Patricia Leal Fernández

Contents

Nomenclature

$\widetilde{*}$	non-dimensional variable of $*$
C_d	drag coefficient per unit length.
C_l	lift coefficient per unit length.
D	cylinder/s diameter (characteristic length L_c).
G	gap between the cylinder and the wall.
L	center-to-center longitudinal spacing between the cylinders in the tandem configuration.
L_x	domain length in the x direction.
L_y	domain length in the y direction.
Re	Reynolds number.
Re_D	Reynolds number based on the diameter of the cylinder.
St	Strouhal number.
U_∞	free stream velocity (characteristic velocity U_c).
x	spatial coordinate in the horizontal direction.
y	spatial coordinate in the vertical direction.

Chapter 1

Introduction & Scope

1.1 Motivation

Throughout history, there are many engineering failures or flaws in the design that occur without being expected or accounted for (fail-safe design) because they are the result of counter-intuitive behavior. Eventually, the inability to predict these phenomena can have undesirable consequences. Some of these failures are surpassed with a design based on trial and error. However, it is more interesting to try understanding the cause, isolating the physics behind the failure event. This project is driven by the latter option. In particular, the project is focused on understanding the physics behind the cross-flow over two tandem circular cylinders in proximity to a plane wall.

The fluctuation of the forces suffered by a body (or group of bodies) immersed in a fluid subjects it to fatigue, which may shorten the life of the structure beyond what was initially estimated. Moreover, fluctuations in the forces may reach the natural frequency of the structure, causing increasing vibrations in amplitude until the destruction of the structure. Acoustic noise can also be an issue for some applications where excessive noise is unacceptable.

The relevance of the present study lies in the frequent appearance of cylindrical structures in air and water mediums (wind and currents, respectively) with wake and proximity interference (related to the location of the downstream cylinder with respect to the upstream cylinder).

Figure 1.1: Left: A350 Main Landing Gear retracting. Source: Daher-Socata || Right: underwater pipeline. Source: Elara Systems [1]

Particularly, an example of cylinders in air flow are the struts and the wheels of the nose landing gear and main landing gear of certain aircraft. When deployed, the nose landing gear sheds periodic vortices. Upon impact with any structure, the flow would induce undesirable vibrations. The critical point occurs when the main landing gear is extending or retracting, the doors of the main landing gear are fully open and the wheel-door distance is minimum (see *figure 1.1 left*). When the nose landing gear vortices impact on the doors, the actuators in charge of opening and closing them suffer many cycles of great amplitude. This reduces significantly the life of the actuators as they suffer fatigue failure sooner than expected. The consequences of this event are not only economical (e.g. maintenance costs, more frequent replacements, etc.), they are also a safety issue.

As for applications in water flow, there are pipes underwater carrying different kinds of fluid substances through them, some of them toxic (e.g. petroleum, gas, etc.). Therefore, the design of the pipes for this application must ensure that the contents are not leaked to the environment. The presence of currents in the oceans and rivers make the arrangement of the pipes (distance to the ground and between pipes) critical to avoid fluctuations in the forces that may compromise the structure (see *figure 1.1 right*).

Aside from the particular examples mentioned above, there are many more practical applications involving flow around cylindrical structures, such as: offshore risers, bridge piers, periscopes, chimneys, towers, masts, stays, cables, antennae and wires (C. Norberg 2003 [2]), which make this topic an attractive choice in terms of scientific investigation.

In this project, the topic involves alternate vortex shedding from a cylindrical body of circular cross section (also known as Von Karman vortex street) and the complex flow patterns formed when interacting with other bodies and/or the proximity to a plane wall. Vortex shedding takes place when the Reynolds number goes past the critical value of the flow moving past a particular body. The Reynolds number mathematical expression is

$$Re = \frac{U_c L_c}{\nu}. \tag{1.1}$$

, where L_c is the characteristic length of the cylinder/s, U_c is the characteristic free stream velocity and ν is the fluid kinematic viscosity.

A clear representation of what has been described above can be found in nature in *figure 1.2.*

There are many factors and parameters that are accountable for the flow field characteristics of flow past cylindrical bodies: distance with respect to other objects or walls, shape of the object/s, arrangement of bodies, Reynolds number, etc.

In *Section 1.2 State of the art*, a brief compilation of previous research on this topic will be mentioned to introduce the reader into the latest developments.

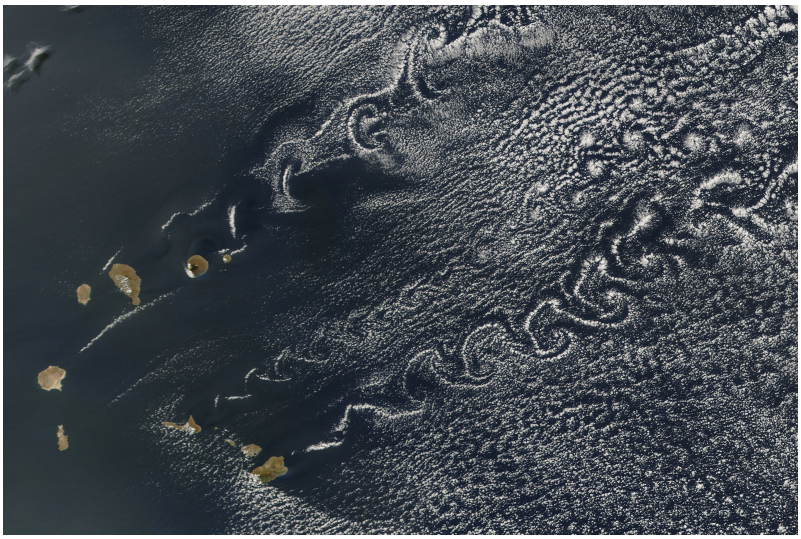

Figure 1.2: Vortices shed by the Cape Verde Islands. Source: University of Washington. Department of atmospheric sciences [3].

1.2 State of the art

Several reviews have been published in the last 10 years that are related to the topic of this project, summarizing the current understanding on the subject of flow around an array of cylinders. This indicates the interest and relevance the topic has for the scientific community. The most relevant review is the one by Sumner [4] and will be cited throughout this section.

Most simulations that handle complex flows have only been validated for low Reynolds numbers. In the case of 2D flow around an array of cylinders in the proximity of a wall, the validity of the condition of bi-dimensional flow has a limitation in the range of Reynolds that can be utilized ($Re < 200 - 300$ [5]).

Nevertheless, numerical simulations have an important advantage with respect to experimental studies on the measurement of forces and other flow characteristics (e.g. Strouhal number, vorticity, etc.). The measurement system on simulations is cheaper and does not disrupt the flow with the presence of equipment. Moreover, even if the quantitative results of a simulation can not be certified, qualitative tendencies can still be relevant to understand the problem.

1.2.1 Tandem configuration

The type of configuration of the pair of cylinders in the present problem is called tandem or in-line configuration, where the cylinders are arranged parallel to the incoming flow (see *figure 1.3*).

It can be inferred from *figure 1.4* that the tandem configuration is in the wake interference region. A body is in the wake interference region when it is partially or completely submerged in the wake of another body. The wake of the upstream cylinder changes the incoming flow characteristics of the downstream cylinder. In turn, the

downstream cylinder alters the wake dynamics and vortex formation of the upstream cylinder [4].

The consequences of the mutual interference between the two cylinders on their behavior can vary depending on the flow conditions, longitudinal distance from center to center, etc.

For isolated cylinders, the upstream cylinder can behave as a turbulence generator and the downstream cylinder as a "drag-reduction" device (counter-intuitive behavior for blunt bodies). Together, the two isolated cylinders form certain flow patterns observed numerically (*figure 1.5*) and experimentally (*figure 1.6*).

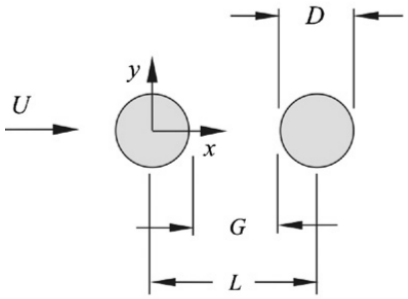

Figure 1.3: Two circular cylinders in cross-flow arranged in tandem. Figure taken from [4]

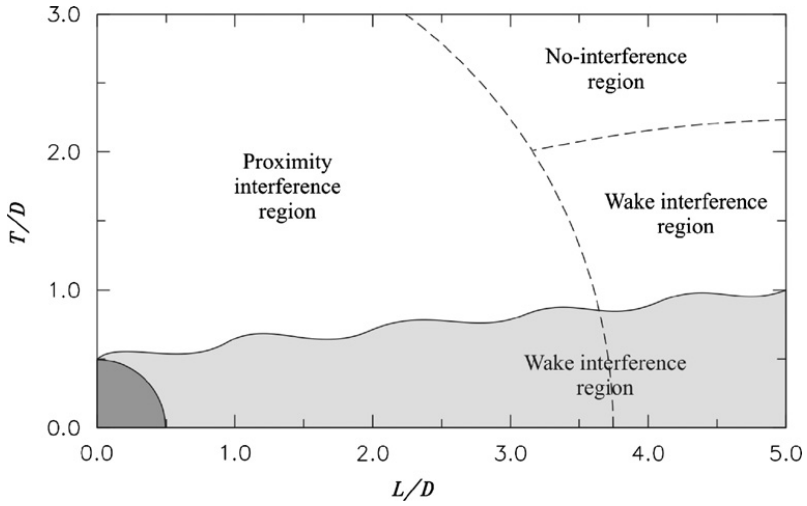

Figure 1.4: Wake and proximity interference boundaries (referenced to the location of the downstream cylinder relative to the upstream cylinder) for two staggered circular cylinders of equal diameter immersed in steady cross-flow, based on Zdravkovich [6]. Figure taken from [4].

Flow patterns of two cylinders of equal diameter in tandem configuration

The classification of flow patterns as a function of the Reynolds number and the longitudinal pitch ratio $^{L}/_{D}$ (the most relevant identified parameters) yields three basic types

of wake interference flow patterns [4]:

- **"Single bluff-body" or "extended-body" regime**: at small values of L/D (see *figure 1.5* and pattern A of *figure 1.6*), the two cylinders behave as if they were a single structure. The downstream cylinder is situated inside the vortex formation region of the upstream cylinder [7], where it is enclosed by the shear layers from the upstream cylinder without reattaching onto its surface. Afterwards, vortex shedding occurs behind the downstream cylinder. At the space between the two cylinders, there can either be stagnant fluid [8], or some oscillatory cavity-flow-type behavior [9].

- **Shear layer reattachment regime**: at intermediate values of L/D (see *figure 1.5* and patterns G, B, C, D, E and E' of *figure 1.6*), the separated free shear layers from the upstream cylinder reattach to the downstream cylinder while no longer enclosing it. At the space between the cylinders there is formation and shedding of eddies[1]. Although many studies have been performed, the fluid behavior in this regime is not completely understood due to the intermittent variation in the properties of the eddies (strength, asymmetry, etc.). In this regime, there is no vortex shedding from the upstream cylinder.

- **"Co-shedding" regime**: at large values of L/D (see *figure 1.5*), the separation between the cylinders is enough so that the downstream cylinder is outside the vortex formation region of the upstream cylinder, and both cylinders experience vortex shedding. The critical L/D at which vortex shedding starts to occur from the upstream cylinder varies depending on the Reynolds number.

1.2.2 Circular cylinders in the proximity of a plane wall

The presence of a wall near an array of cylinders influences the forces that appear in the bodies in an asymmetric way, creating even more complex geometries than those observed for isolated cylinders. The effects induced by the distance from the bodies to the wall are not fully understood. Proof of that is the future work proposed by Sumner [4], who stresses the need for further study on the tandem configuration for the condition of plane wall proximity.

[1] An eddy is a circular current of water [10], or in a more general sense, a circular current of fluid.

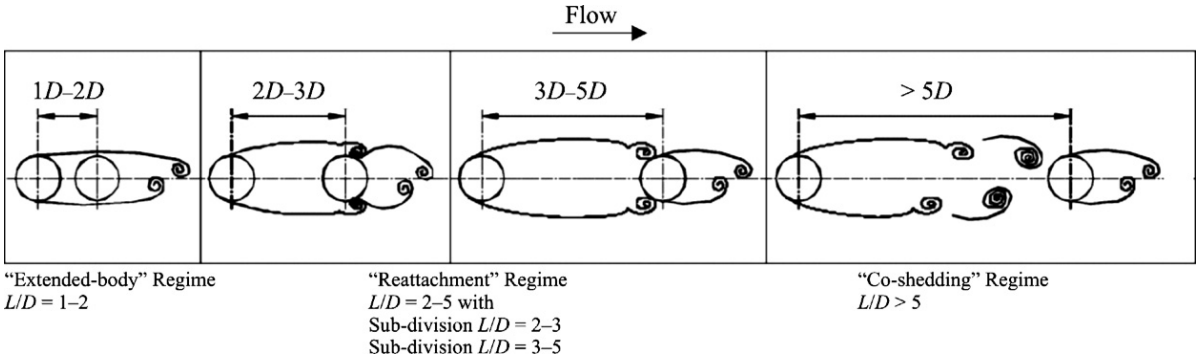

Figure 1.5: Simplified classification scheme of the flow patterns for two tandem circular cylinders in cross-flow, from [11] and [12], as a function of Reynolds number. Figure taken from [4]

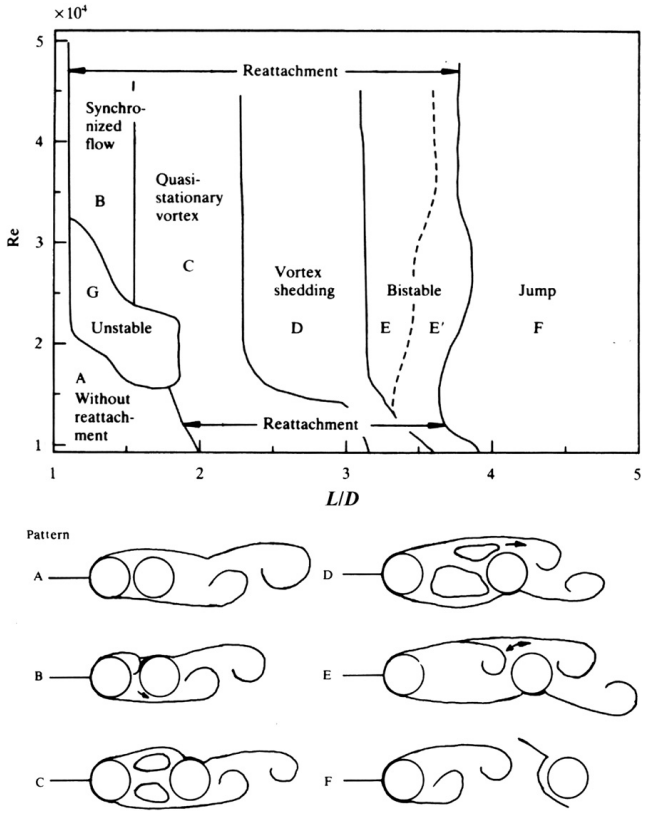

Figure 1.6: Classification of flow patterns for two tandem circular cylinders in cross-flow, from [13], as a function of the longitudinal center-to-center pitch ratio and Reynolds number. Figure taken from [4]

Chapter 2

Objectives

Along with serving the intrinsic purpose of a bachelor thesis, the main objective of this project is to understand the forces that appear in an array of cylinders (tandem configuration) in the presence of a plane wall[1]. In particular, the differences in the amplitude and frequency of the forces acting on the first and second cylinders will be assessed.

An actual solid plane wall imposes a no-slip boundary condition to the fluid. This condition can be separated into two effects: a **velocity gradient** and a **confinement effect** (the proximity of the cylinder to the wall produces a blockage effect that influences the forces acting on the cylinder/s).

This project focuses on the study of the confinement effect, separated from the velocity gradient, with the objective of understanding the proximity interference of an actual solid plane wall. The confinement effect is uncoupled from the velocity gradient by setting the boundary condition on the sides of the domain as free-slip (see *Section 3.3.1 Boundary Conditions*).

Furthermore, the effects of several parameters involved in the problem configuration will be evaluated; the effect of gap (changing the values from isolated to $^{G}/_{D} = 1$ and $^{G}/_{D} = 0.25$), the effect of the longitudinal separation between the cylinders ($^{L}/_{D} \to \infty$, $^{L}/_{D} = 2$ and $^{L}/_{D} = 4$) and the effect of Reynolds number ($Re = 100$ and $Re = 200$).

[1]This document refers to the term *wall* as the free-slip boundary condition on the sides of the domain (excluding the inlet and outlet), unless explicitly indicated (see *figure 3.1*.

Chapter 3

Problem modeling

The next step is to define the complete problem to be solved. The combination of the concepts sketched during previous chapters, along with defining the boundaries and simplifications, will shape the mathematical model that intends to represent the physical reality of the flow around an array of cylinders.

The general outlook of the problem can be characterized by the following remarks:

- The geometry of the bodies consists in 2D circular cylinders of equal diameter D.
- The geometry of the computational domain is rectangular (see *figure 3.1*). It can have different dimensions L_x and L_y depending on the configuration of the parameters (i.e. isolated or in the proximity of a plane wall). When the cylinder/s are considered to be isolated, it means the vertical spacing to the lateral walls of the domain is enough to not influence their behavior. The value of the gap for this condition is $^G/_D = 14$.

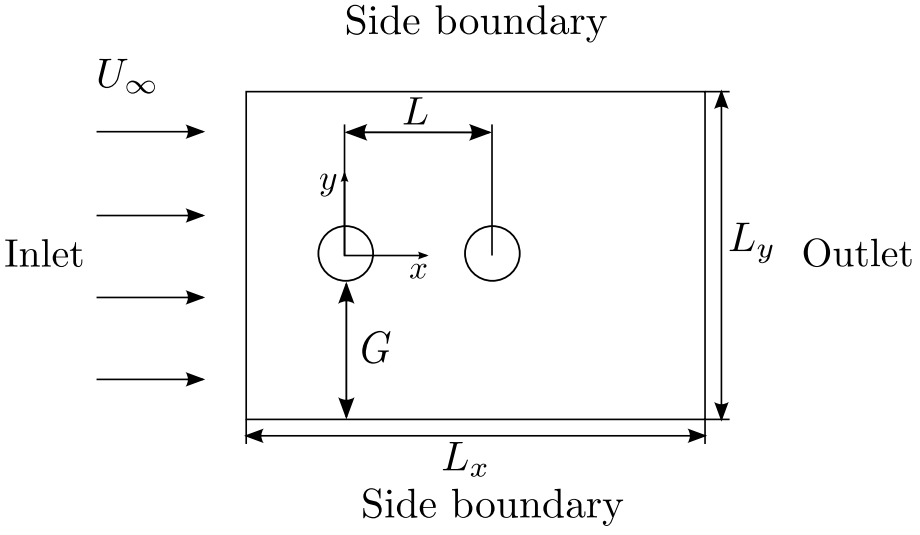

Figure 3.1: Simplified domain and problem configuration.

- Different set of configurations (see *section 4.3 Work plan*) result from the combination of the subsequent parameters:

- Single ($^{L}/_{D} \to \infty$) or pair of cylinders in tandem.
- Longitudinal spacing between the cylinders: $^{L}/_{D} = 2$ or $^{L}/_{D} = 4$.
- Vertical spacing between the cylinder/s and the plane wall: $^{G}/_{D} = 14$, $^{G}/_{D} = 1$ or $^{G}/_{D} = 0.25$.
- Reynolds number: $Re = 100$ or $Re = 200$.

To obtain the results on the present fluid dynamics problem, the incompressible 2D unsteady Navier-Stokes equations for a Newtonian fluid will be solved numerically.

3.1 Basic assumptions

Prior to stating the mathematical model, a series of assumptions are taken into account to simplify the expression of the equations to be solved (see *section 3.2 Governing equations*):

- The fluid is incompressible (i.e. constant density). For this assumption to be valid, the Mach number must be sufficiently small

$$M_\infty = \frac{U_\infty}{a} \ll 1 \tag{3.1}$$

, where a is the speed of sound. For the case of underwater pipelines in seawater, the speed of sound is approximately $a = 1500\ ^{\mathrm{m}}/_{\mathrm{s}}$ [14] (it depends on salinity and other factors), and the average speed in the westward flowing South Equatorial current (the area where the Cape Verde Islands are located, see *figure 1.2*) $U_\infty = 9\ ^{\mathrm{km}}/_{\mathrm{h}} = 2.5\ ^{\mathrm{m}}/_{\mathrm{s}}$ [15]. This yields $M_\infty = 0.001\widehat{6} \ll 1$. The advantage of considering an incompressible fluid is that wave propagation does not occur, allowing for bigger time steps Δt.

- The fluid is Newtonian (i.e. constant viscosity).
- The flow is two-dimensional. This means that the chosen geometry (circular cylinder) can be projected into a plane perpendicular to the axis of the cylinder without losing information about the body. Another important feature to fulfill two-dimensionality is that the boundary conditions must be contained within the plane where the geometry is projected. This implies as well that the span of the cylinders must be infinite. Otherwise, the information at either end of the cylinders would not be taken into account. The validity of the assumption needs to be complemented by sufficiently low Reynolds numbers ($Re < 200 - 300$ [5]).
- The temperature is uniform throughout the computational domain. In addition, the incompressible Navier-Stokes equations of continuity and momentum are uncoupled from the energy equation. Thus, the project will focus on the mechanical problem, removing the energy equation from the governing equations.
- Gravitational forces $\vec{g}$ are negligible. They are important only in boundary layers where fluid buoyancy is dominant.
- The cylinder or pair of cylinders are fixed and infinitely rigid.

3.2 Governing equations

For the incompressible problem, the 2D Navier-Stokes equations consist of a time-dependent continuity equation (3.2) for conservation of mass, two time-dependent momentum conservation equations (3.3) and (3.4), and a time-dependent conservation of energy equation.

In the complete system of equations, there are three independent variables and five dependent variables. The independent variables are the x and y spatial coordinates of the domain and the time t. The dependent variables are the pressure p, density ρ, and temperature T (which is contained in the energy equation through the total energy), and two components of the velocity vector; the u component in the x direction and the v component in the y direction [16]. The energy equation is not studied in this problem because it is uncoupled from the continuity and momentum equations, and does not add value to the objectives of the project.

Continuity equation:

$$\frac{\partial \rho}{\partial t} + \frac{\partial (\rho u)}{\partial x} + \frac{\partial (\rho v)}{\partial y} = 0 \tag{3.2}$$

Momentum equation in the x direction:

$$\left(\frac{\partial \rho u}{\partial t} + \frac{\partial \rho u^2}{\partial x} + \frac{\partial \rho uv}{\partial y}\right) = -\frac{\partial p}{\partial x} + \mu\left(\frac{\partial^2 u}{\partial x^2} + \frac{\partial^2 u}{\partial y^2}\right) + \rho g_x \tag{3.3}$$

Momentum equation in the y direction:

$$\left(\frac{\partial \rho v}{\partial t} + \frac{\partial \rho uv}{\partial x} + \frac{\partial \rho v^2}{\partial y}\right) = -\frac{\partial p}{\partial y} + \mu\left(\frac{\partial^2 v}{\partial x^2} + \frac{\partial^2 v}{\partial y^2}\right) + \rho g_y \tag{3.4}$$

, where the g terms are the components of the gravity body forces.

Looking at equations (3.2), (3.3) and (3.4), it is noticeable that the dependent variables appear in each one. The consequence of this event is that the system of equations is coupled and the equations have to be solved simultaneously. The coupled system of equations can be solved using a fractional step method described by Brown [17]. The method involves two actions for each time step. The first action is to advance in time with the time information from the momentum equations without taking into account the condition imposed by the continuity equation. Afterwards, the continuity equation must be fulfilled implicitly.

For incompressible Newtonian fluids, the continuity and momentum equations in Cartesian coordinates (x, y), in the absence of gravitational forces, reduce to:

$$\frac{\partial u}{\partial x} + \frac{\partial v}{\partial y} = 0 \tag{3.5}$$

$$\rho\left(\frac{\partial u}{\partial t} + \frac{\partial u^2}{\partial x} + \frac{\partial uv}{\partial y}\right) = -\frac{\partial p}{\partial x} + \mu\left(\frac{\partial^2 u}{\partial x^2} + \frac{\partial^2 u}{\partial y^2}\right) \tag{3.6}$$

$$\rho\left(\frac{\partial v}{\partial t} + \frac{\partial uv}{\partial x} + \frac{\partial v^2}{\partial y}\right) = -\frac{\partial p}{\partial y} + \mu\left(\frac{\partial^2 v}{\partial x^2} + \frac{\partial^2 v}{\partial y^2}\right) \tag{3.7}$$

The code used to obtain the solution and post-processing the results works with non-dimensional variables and parameters. The non-dimensional expression of the reduced set of Navier-Stokes equations is achieved using the diameter of the cylinders D as characteristic length, and the free stream uniform velocity U_∞ as the characteristic velocity:

$$\frac{\partial \tilde{u}}{\partial \tilde{x}} + \frac{\partial \tilde{v}}{\partial \tilde{y}} = 0 \tag{3.8}$$

$$\frac{\partial \tilde{u}}{\partial \tilde{t}} + \frac{\partial \tilde{u}^2}{\partial \tilde{x}} + \frac{\partial \tilde{u}\tilde{v}}{\partial \tilde{y}} = -\frac{\partial \tilde{p}}{\partial \tilde{x}} + \frac{1}{Re}\left(\frac{\partial^2 \tilde{u}}{\partial \tilde{x}^2} + \frac{\partial^2 \tilde{u}}{\partial \tilde{y}^2}\right) \tag{3.9}$$

$$\frac{\partial \tilde{v}}{\partial \tilde{t}} + \frac{\partial \tilde{v}^2}{\partial \tilde{y}} + \frac{\partial \tilde{u}\tilde{v}}{\partial \tilde{x}} = -\frac{\partial \tilde{p}}{\partial \tilde{y}} + \frac{1}{Re}\left(\frac{\partial^2 \tilde{v}}{\partial \tilde{x}^2} + \frac{\partial^2 \tilde{v}}{\partial \tilde{y}^2}\right) \tag{3.10}$$

, where $\tilde{x} = \frac{x}{D}$ is the non-dimensional horizontal coordinate, $\tilde{y} = \frac{y}{D}$ is the non-dimensional vertical coordinate, $\tilde{u} = \frac{u}{U_\infty}$ is the non-dimensional velocity in the x direction, $\tilde{v} = \frac{v}{U_\infty}$ is the non-dimensional velocity in the y direction, $\tilde{t} = t\frac{U_\infty}{D}$ is the non-dimensional time and $\tilde{p} = \frac{p}{\rho {U_\infty}^2}$ is the non-dimensional pressure.

From the analysis of the Navier-Stokes equations in non-dimensional form, it can be observed that the only parametric dependence of the equations is the Reynolds number.

3.3 Computational domain

The computational domain of the problem is discretized using a uniform Cartesian staggered grid, independent of the body geometry. The domain is split into cells, where n_x and n_y are the number of cells in the x and y direction, respectively. Staggered grid means that the points where the pressure p, the horizontal velocity u_x and the vertical velocity u_y are computed are not the same point (see *figure 3.2*). The grid is uniform if the spacing between cells is the same in the x and y direction (i.e. $dx = dy$).

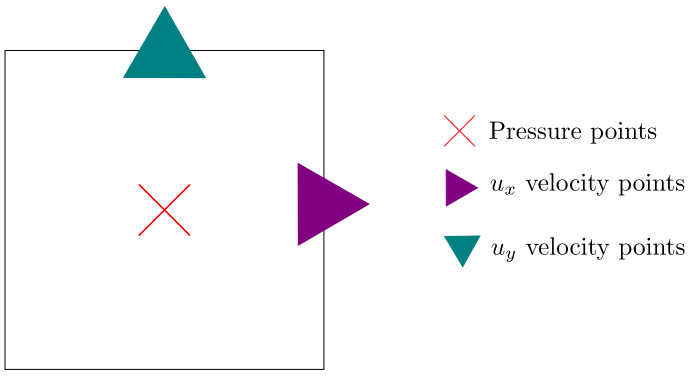

Figure 3.2: Example of a grid cell ij.

3.3.1 Boundary Conditions

The following boundary conditions establish the kind of problem to be solved (i.e. flow specifications, domain restrictions, etc). The boundary conditions at the sides of the

computational domain (inlet, outlet and lateral walls) have to be chosen carefully, especially the outlet. The dimensions of the computational domain are restrictive in terms of CPU time and computational costs. The chosen dimensions are the smallest that allow minimum flow interference without losing accuracy. The shape of the domain is rectangular and the dimensions vary depending on the case studied (isolated or near a wall).

- Uniform free stream at the inlet:

$$u = U_\infty \tag{3.11}$$

$$v = 0 \tag{3.12}$$

- Convective boundary condition at the outlet:

$$\frac{\partial u}{\partial t} + C\frac{\partial u}{\partial x} = 0 \tag{3.13}$$

, where C is the convective velocity, calculated to fulfill conservation of mass for an incompressible fluid (i.e. it is the velocity required to make the outflow mass flux equal to the incoming mass flux) [18].

- Free-slip boundary conditions for the lateral walls of the domain:

$$\frac{\partial u}{\partial y} = 0 \tag{3.14}$$

$$v = 0 \tag{3.15}$$

The general outline of the rectangular domain is displayed in the following *figure*:

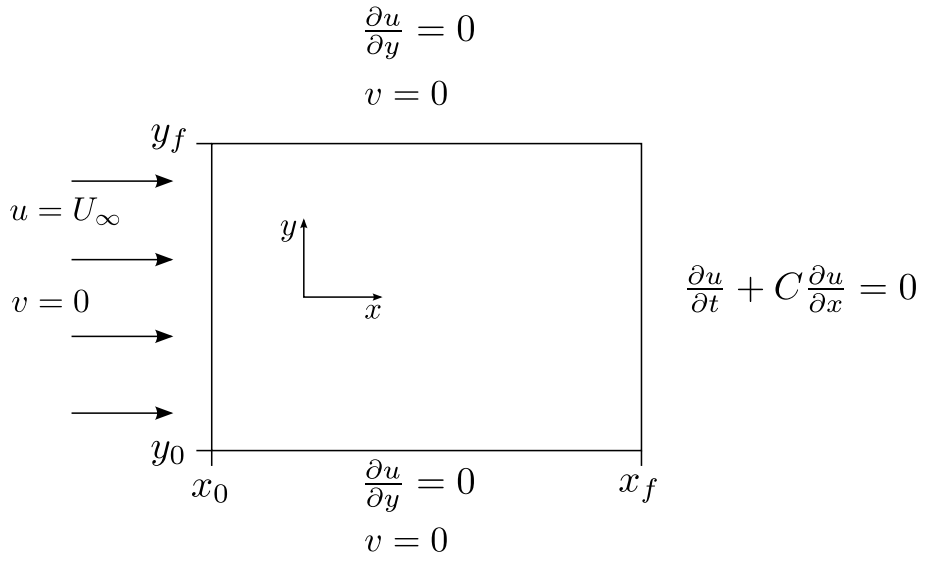

Figure 3.3: Outline of the domain with boundary conditions and reference system.

, where x_0 and x_f are the limits of the domain in the x direction, and y_0 and y_f are the limits of the domain in the y direction.

- No-slip condition at the surface of the cylinders.

The following sections intend to discuss and justify the motivation that led to the final selection of key parameters for the configuration of the problem.

3.4 Courant–Friedrichs–Lewy condition

Numerical simulations based on partial differential equations require spatial and temporal discretization. The temporal discretization is carried out performing the integration of every term in the differential equations over the time step, $\triangle t$. A consequence to performing an explicit time integration[1] (e.g. Euler's method) is that there is a critical time step for the numerical scheme to be stable and converge to the solution. The critical time step is given by the Courant-Friedrichs-Lewy (CFL) condition.

The following mathematical expression is the application of the CFL condition in one dimension:

$$CFL = \frac{U \triangle t}{\triangle x} \leq CFL_{max} \tag{3.16}$$

, where CFL is the non-dimensional parameter called Courant number, U represents the largest velocity in the system, $\triangle t$ is the time step and $\triangle x$ the cell size.

Depending on the integration scheme performed, the Courant number CFL_{max} has a different value to guarantee a stable solution. For the present problem, the solution advances in time using a three-step low-storage semi-implicit Runge-Kutta scheme, which imposes the theoretical limit $CFL \leq \sqrt{3}$.

The physical interpretation of the CFL condition for a fluid mechanics problem is that, if $CFL > CFL_{max}$ the fluid particles are traveling two or more cells per time step Δt. Therefore, the time step must be smaller than the time it takes for the fluid particle to travel to adjacent grid points.

This is only a summary to introduce the notion of the Courant number and the CFL condition to the reader. A deeper understanding is out of the scope of this project. However, further information on this topic can be found in [19].

Once considered the CFL condition applicable to the present problem, a conservative value of $CFL = 0.6$ was initially chosen. However, this value is not the definitive due to the non-convergence of the mean value of the drag coefficient, found during the refinement of the grid resolution (see *figure 3.4*). Therefore, the discussion on the selection of the CFL parameter continues in *section 3.5 Grid refinement study*.

3.5 Grid refinement study

Setting the number of points in the mesh to large values yields more accurate results. On the other hand, a greater number of points increases the computational cost of the simulations. Consequently, a trade-off was made to obtain the lowest resolution possible without compromising the accuracy of the results.

The study consisted in running several simulations for the case of an isolated single cylinder with a square domain (the domain size is $28Dx28D$), keeping all the parameters constant except the resolution of the grid. Since the exact value of the results is not known beforehand, the criteria for choosing the appropriate resolution is to compare the results between two different grids. If the changes in magnitude are within the tolerance

[1] Explicit time integration calculates the future state of a system at a time $t + \Delta t$ based on the solution at the current time step t.

range (1% difference), the lowest resolution between the two is chosen. If the condition is not met, further refinement is necessary.

Figure 3.4 shows the comparison between C_l and C_d for four different grid resolutions ($^n/_D \simeq 19,\ 37,\ 74,\ 147$[2]). After evaluating the results, convergence is achieved for the lift coefficient and the standard deviation (RMS) of the drag coefficient for $^n/_D \simeq 37$. In spite of the evident vertical displacement between the curves, the difference is still less than 1%. It represents the mean value of the drag coefficient. Although the difference is sufficiently small, the fact that improving the resolution did not reduce the separation between the curves raised questions that motivated a parallel investigation in the department.

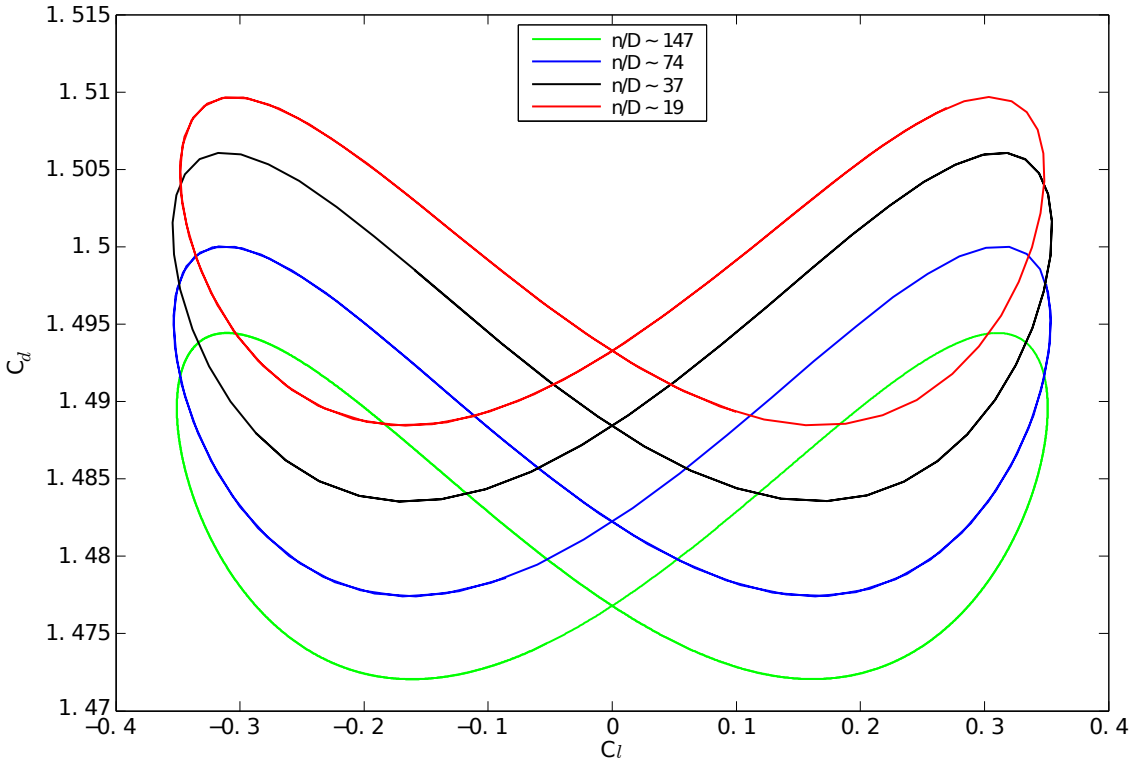

Figure 3.4: Lift coefficient vs. Drag coefficient for different grid resolutions.

The findings of the investigations led to selecting a grid with $^n/_D = 64$ and lowering the CFL to 0.15.

To explain the cause for the event observed in *figure 3.4*, some aspects of the immersed boundary method (IBM) and the numerical scheme need to be introduced.

The IBM simulates the presence of the body in the flow, modeled as a series of points that conform the shape of the surface. At each point, a forcing term $\vec{f}$ is introduced in the momentum equation to fulfill the no-slip condition at the surface of the cylinder. In broad terms, the complete algorithm for the numerical simulation is solved in several steps every Δt (fractional step method). Part of the numerical process is to calculate the forces on the surface of the body at a certain Δt. After this step, it is necessary

[2]The values are indicated as approximate because the exact results are rational numbers resulting from selecting $n_x = n_y = 512,\ 1024,\ 2048,\ 4096$ and $L_x = L_y = 28D$.

to do pressure corrections to implicitly fulfill the continuity equation (3.8). This step introduces a friction error on the surface of the cylinders proportional to $\frac{\Delta t}{Re}$. Since the Reynolds number for the simulations is small, Δt must be very small in order to minimize the friction error.

Recalling the expression of the CFL:

$$CFL = \frac{U \triangle t}{\triangle x}$$

Hence, lowering the CFL decreases the value of Δt. By selecting the appropriate value of the CFL, in this case $CFL = 0.15$, the friction error becomes small enough and the mean value of the C_d converges successfully.

3.6 The Reynolds number and the two-dimensional condition

At the beginning of the project the boundaries between low and moderate Reynolds number were not clearly defined, so the value was initially set to $Re = 500$. After analyzing the visualization of the flow, an anomaly was observed in the vorticity contour for the case of a single isolated cylinder with $Re = 500$ (see *figure 3.5*). In the domain outlet, part of the flow appeared to be circulating backwards, in the direction opposing the free stream.

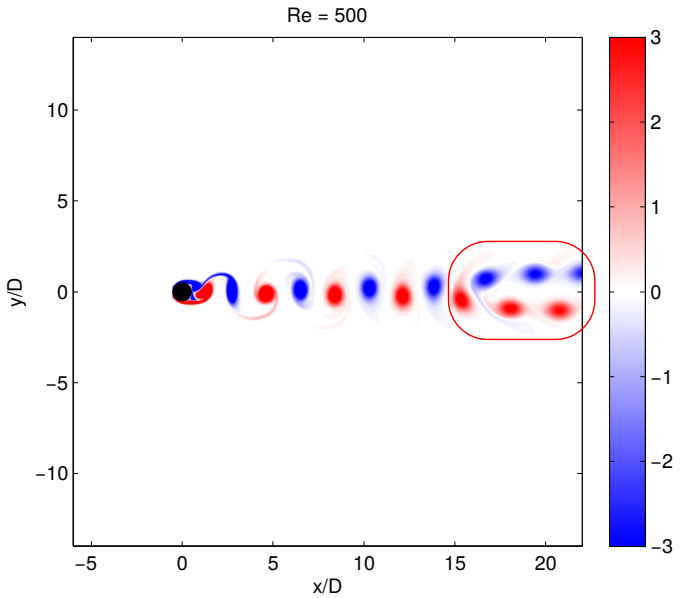

Figure 3.5: Vorticity contour for an isolated single cylinder. Domain size: $28Dx28D$.

The first educated guess was that the outlet boundary condition interfered with the flow, instead of letting it move freely out of the domain. To confirm or discard that the outlet was interfering with the flow, a study parallel to the project was carried out.

The study consisted on enlarging the computational domain in the horizontal direction and evaluating the vorticity contours. After a few tests, it was concluded that the

outlet condition was not responsible for the behavior downstream, because the anomaly started at the same $^{x}/_{D}$ position regardless of the distance to the outlet boundary (see *figure 3.6*).

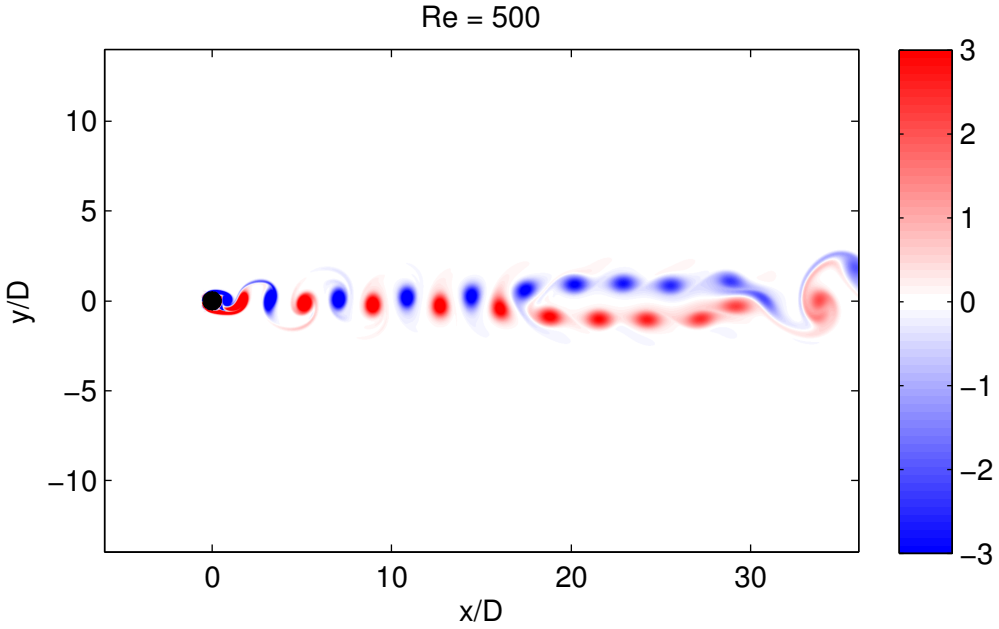

Figure 3.6: Vorticity contour for an isolated single cylinder. Domain size: $36Dx28D$.

A second review to the literature lead to the conclusion that the Reynolds number was too high and the flow was not two-dimensional. The code tried to adapt a flow with 3D characteristics to what is observed in *figure 3.5* and *3.6*.

The solution was to set the Reynolds number to lower values ($Re = 100, 200$) to fulfill the condition for 2D flow (see *3.1 Basic assumptions*).

Chapter 4

Methodology

In order to carry out the research and fulfill the objectives proposed in *Chapter 2*, a set of tools and a structured planning are required.

Subsequent sections on this chapter will briefly present the software, hardware and work plan to give the reader an idea of the methodology followed throughout the project.

4.1 Software

The software is the main tool of the project. It is necessary to pre-process and run the simulations, as well as post-process the output results.

The creation of the geometry of the cylinders and the post-processing of the output is handled by the commercial software MATLAB®. Some of the functions used within this software were built specifically for the code, in order to handle the binary output generated by the code.

The main software responsible for running the simulations is an in-house code written in F95. The code consists on a basic fluid solver of the incompressible Navier-Stokes equations for a Newtonian fluid, with an immersed boundary approach for the representation of bodies submerged in the fluid.

Navier-Stokes solver

The Navier-Stokes equations are solved numerically by Direct Numerical Simulation (DNS), thus it is not necessary to introduce a turbulence model. The discretization process is performed as follows:

- The temporal scheme treats differently the corresponding linear and non-linear parts of the equations. The linear part is solved implicitly and the non-linear part explicitly.
- The spatial discretization is performed through the second order finite differences method.

Immersed Boundary Method

To simulate the presence of the body, the code implements the Immersed Boundary Method (IBM) described by Uhlmann [20]. This method has the advantage that the

grid of the computational domain does not need to fit the body. As mentioned in *section 3.5 Grid refinement study*, the body is modeled by representing its external surface as a series of points. At each point, a forcing term $\vec{f}$ is introduced in the momentum equation to fulfill the no-slip condition at the surface of the cylinder. The number of points of the body depends on the node density of the grid.

4.2 Hardware

Aside from a personal computer to act as interface for pre-processing the code, launching the simulations and post-processing the data extracted from the simulations, the most important piece of equipment is the computer cluster provided by the University.

The software mentioned in the previous *section 4.1* is accessed through a secure remote connection (*ssh*) to the computer cluster named "*icaro*".

Computer cluster definition [21]: a computer cluster is a group of computers connected to each other through fast local area networks (LAN). This arrangement is called "parallel computing" because the machines work as a single unit. Under most circumstances, clusters are more cost effective than supercomputers in terms of computational speed.

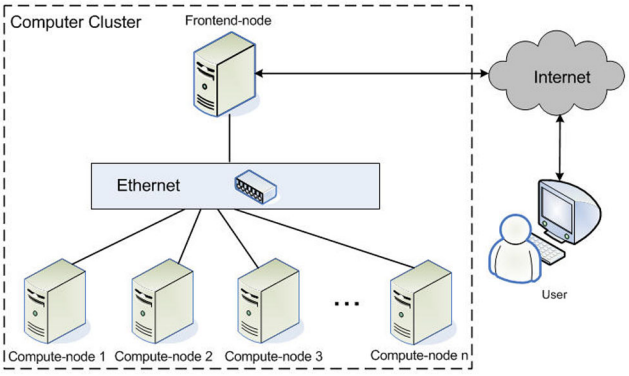

Figure 4.1: Computer Cluster Architecture [22]

Technical description of the cluster for the department of aerospace engineering: 156 cores (26 Intel Xeon X5650 processors), 632GB of total RAM. Cluster connected to two redundant RAID5 systems, with 10TB each.

4.3 Work plan

This section contains a description of the work procedure and the organization of the test cases.

After reviewing the literature and performing the preliminary studies discussed in *Chapter 3 Problem modeling*, the scope of the project was defined.

The combination of the variable parameters of the problem (number of cylinders, longitudinal pitch ration $^{L}/_{D}$, gap ratio $^{G}/_{D}$ and Reynolds number Re), resulted in 18 different problem configurations.

Simulation pre-processing

Once each test case is defined by the parameters, flow conditions, cylinder geometry and boundary conditions, a series of files are created to translate the problem into commands understandable by the code.

1. First of all, a MATLAB file is written to create the geometry of the cylinder or cylinders as a function of the diameter and the spacing between the nodes dx (remember that the grid is uniform so that $dx = dy$). The output of this file is the data of the set of points (in Cartesian coordinates) that conform the surface of the cylinder.

2. Afterwards, the main script that contains the remaining information of the problem is created from a template. In this executable file, the following data parameters are defined[1]:

    - Computer cluster queue requirements: number of computer nodes and processors to be used for the simulation, as well as the identification name of the simulation.
    - Path specification of the directory where the information of the simulation is to be stored.
    - Base-name that unambiguously identifies each case.
    - Restart options to indicate whether the simulation starts from scratch, reads initial conditions and starts a new run or continues working from a previous simulation.
    - Physical parameters: Reynolds number. It was determined in *section 3.2 Governing equations* that the Reynolds number was the only parametric dependence that appeared in the non-dimensional Navier-Stokes equations.
    - Run parameters: time to run the simulation, time to save the information in frames of the solution and the CFL_{max}.
    - Domain specifications: number of nodes n_x and n_y, and domain size bounded by the limits $[x_o, x_f]$ and $[y_o, y_f]$.
    - Path specification of the directory where the geometry data is stored.

3. The final step of the pre-processing is to launch the main script to the queue of the computer cluster to run the simulation. The rest is handled by the software.

Optimization techniques

The convergence of the simulations is achieved when the temporal evolution of the forces produces a signal that is either constant or periodic with a constant value for the mean and amplitude of the force. For the tolerance specified in this project, the difference in amplitude between the maximum (or minimum) of two consecutive periods of the converged case must be less than 1%.

[1] This is not an exhaustive list. There are more lines in the script written by default.

If the simulations had been run from scratch with the optimum grid resolution, they would have taken too long to converge to the solution. Therefore, a strategy was implemented to be more efficient in the convergence of the problem. The subsequent steps describe the process:

1. Converge each case using a coarse grid. This takes significantly less time than higher resolutions.
2. Create a restart file interpolating the results of the low resolution case into the adequate grid resolution.
3. Run the simulation again with the adequate grid, using the restart option of starting a new run from a restart file. At first, the errors of the interpolation need some time to be corrected. After a reasonably short time, the signal meets the convergence standards.

This scheme allows to save a considerable amount of time in each simulation, which is important to achieve computational efficiency considering there are 18 different cases to be run.

Analyzed Cases

To allow for an organized post-processing of the results, the test cases were organized into two main categories:

- Isolated cylinders: the cylinder/s are considered to be isolated when the separation to the lateral boundaries of the domain is $^{G}/_{D} = 14$.
  - Single cylinder.
  - Tandem cylinders with $^{L}/_{D} = 2$.
  - Tandem cylinders with $^{L}/_{D} = 4$.
- Cylinders in the proximity to a plane wall: the cylinder/s are in the proximity to the wall when $^{G}/_{D} = 1$ or $^{G}/_{D} = 0.25$.
  - Single cylinder with $^{G}/_{D} = 1$.
  - Single cylinder with $^{G}/_{D} = 0.25$.
  - Tandem cylinders with $^{G}/_{D} = 1$ and $^{L}/_{D} = 2$.
  - Tandem cylinders with $^{G}/_{D} = 1$ and $^{L}/_{D} = 4$.
  - Tandem cylinders with $^{G}/_{D} = 0.25$ and $^{L}/_{D} = 2$.
  - Tandem cylinders with $^{G}/_{D} = 0.25$ and $^{L}/_{D} = 4$.

These cases are evaluated for $Re = 100$ and $Re = 200$, yielding the 18 different test cases.

Chapter 5

Results

This chapter deals with the presentation and interpretation of the results obtained from the simulations through the analysis of the output. A validation of the present tool for the simplest cylinder arrangement is done to assure that the results comply with other publications that have evaluated the same case, before moving on to more complex geometries.

5.1 Validation of the results

For the purpose of validating the present problem configuration, the compilation by Harichandan et al. [23] of numerical results from several researchers on the flow past a single circular cylinder are compared to the present results. The comparison is presented in *table 5.1.*

	Lift Coefficient		Drag Coefficient		Strouhal Number	
	Re=100	Re=200	Re=100	Re=200	Re=100	Re=200
Braza et al. (1986)	± 0.250	± 0.750	1.364 ± 0.015	1.400 ± 0.050	0.160	0.200
Meneghini et al. (2001)			1.370 ± 0.010	1.300 ± 0.050	0.165	0.196
Ding et al. (2007)	± 0.287	± 0.659	1.356 ± 0.010	1.348 ± 0.050	0.166	0.196
Harichandan et al. (2012)	± 0.278	± 0.602	1.352 ± 0.010	1.320 ± 0.050	0.161	0.192
Present result	± 0.255	± 0.532	1.455 ± 0.008	1.453 ± 0.036	0.173	0.204

Table 5.1: Parameters for the flow past an isolated single circular cylinder.

The present results for the flow past an isolated single circular cylinder show compliance with the data published by other researchers, proving that the present tool is able to solve the flow around a cylinder. Therefore, it can be used to face the problem of an array of cylinders in the proximity of a plane wall.

Table 5.2 contains all the data of the aerodynamic forces and the Strouhal number for all the run simulations. Wherever $^{L}/_{D} = \infty$ is introduced, it refers to the single cylinder case. This table is the principal source of information to analyze and interpret the results, with the aid of flow visualization and graphical representations of the aerodynamic forces and the Strouhal number with the key parameters.

Cylinder arrangement			Lift Coefficient		Drag Coefficient		Strouhal number	
			Re=100	Re=200	Re=100	Re=200	Re=100	Re=200
G/D = 14	L/D = ∞		± 0.255	± 0.532	1.455 ± 0.008	1.453 ± 0.036	0.173	0.204
	L/D = 2	1st	± 0.004	± 0.024	1.272 ± 0.000	1.133 ± 0.000	0.129	0.140
		2nd	± 0.016	± 0.116	−0.104 ± 0.000	−0.218 ± 0.002	0.129	0.140
	L/D=4	1st	± 0.331	± 0.611	1.396 ± 0.019	1.407 ± 0.044	0.155	0.188
		2nd	± 1.090	−0.001 ± 1.496	0.813 ± 0.164	0.622 ± 0.191	0.155	0.188
G/D = 1	L/D = ∞		0.136 ± 0.403	0.097 ± 0.725	1.729 ± 0.029	1.698 ± 0.055	0.196	0.222
	L/D = 2	1st	0.120 ± 0.049	0.067 ± 0.090	1.527 ± 0.007	1.375 ± 0.014	0.160	0.173
		2nd	0.082 ± 0.182	0.080 ± 0.411	0.115 ± 0.035	0.010 ± 0.091	0.160	0.173
	L/D=4	1st	0.148 ± 0.459	0.117 ± 0.735	1.629 ± 0.048	1.575 ± 0.068	0.177	0.201
		2nd	0.008 ± 1.367	0.014 ± 1.483	0.821 ± 0.176	0.557 ± 0.172	0.177	0.201
G/D = 0.25	L/D = ∞		0.520 ± 0.004	0.430 ± 0.621	1.625 ± 0.002	1.875 ± 0.208	0.131	0.200
	L/D = 2	1st	0.448 ± 0.000	0.373 ± 0.009	1.597 ± 0.000	1.480 ± 0.009	—	0.131
		2nd	0.172 ± 0.000	0.114 ± 0.245	0.226 ± 0.000	0.144 ± 0.099	—	0.131
	L/D=4	1st	0.506 ± 0.000	0.408 ± 0.000	1.575 ± 0.000	1.370 ± 0.000	—	0.105
		2nd	0.177 ± 0.000	0.157 ± 0.020	0.249 ± 0.000	0.179 ± 0.010	—	0.104

Table 5.2: Flow parameters for the complete set of test cases.

5.2 Sensitivity to gap ratio

The visualization of the flow in *figures 5.1, 5.2* and *5.3* through the vorticity contours is a useful resource for the qualitative study of the simulations and the identification of the flow patterns in the tandem configurations.

The pair of cylinders in tandem with a longitudinal separation of $^{L}/_{D} = 2$ behave as a single bluff body for every value of the gap ratio.

For the two cylinders in tandem with $^{L}/_{D} = 4$, the flow pattern corresponds to the shear-layer reattachment regime for every gap ratio except for $^{G}/_{D} = 0.25$, where it resembles the flow pattern of the extended-body regime.

For all the configurations of tandem cylinders, the drag coefficient is higher for the first cylinder because the second is shielded from the incoming flow. The value of the drag on the second cylinder is affected mostly by the longitudinal separation between the cylinders and the gap ratio.

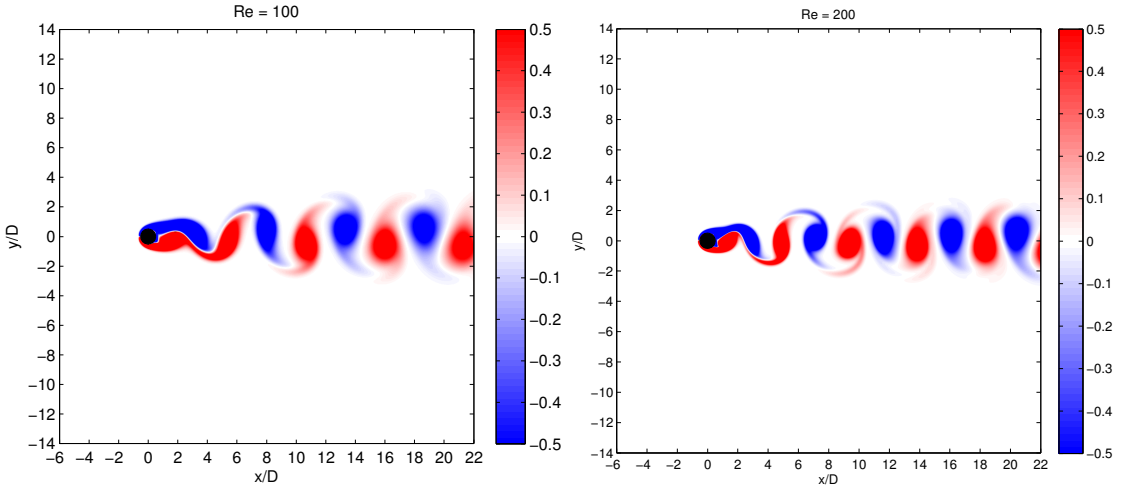

(a) Single cylinder.

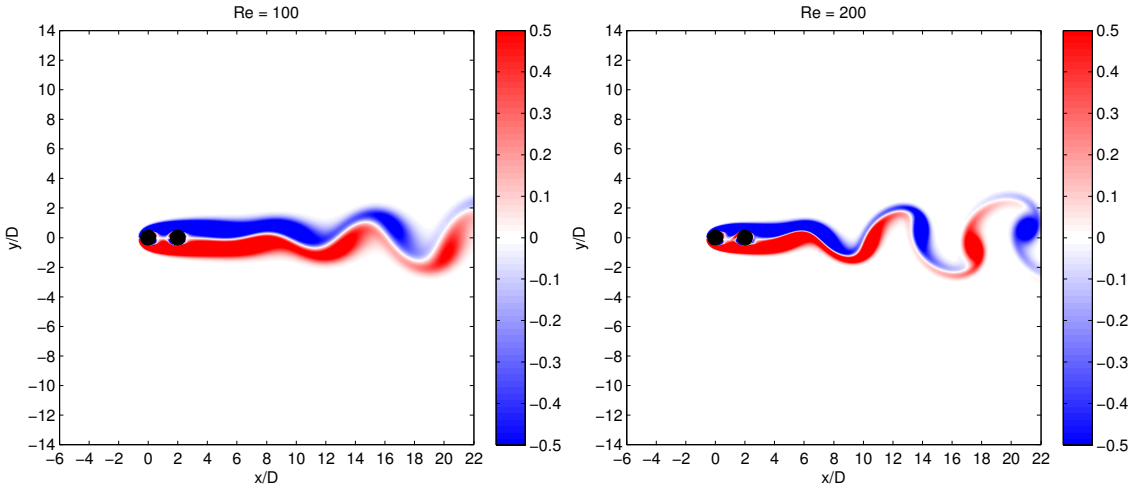

(b) Two tandem cylinders with $^{L}/_{D} = 2$.

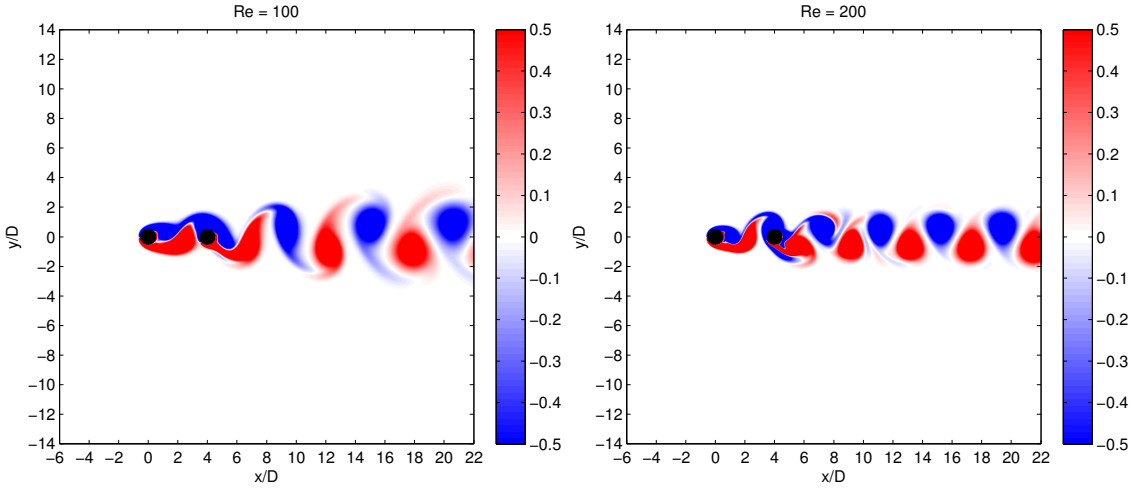

(c) Two tandem cylinders with $^{L}/_{D} = 4$.

Figure 5.1: Vorticity contours for $^{G}/_{D} = 14$ (Isolated)

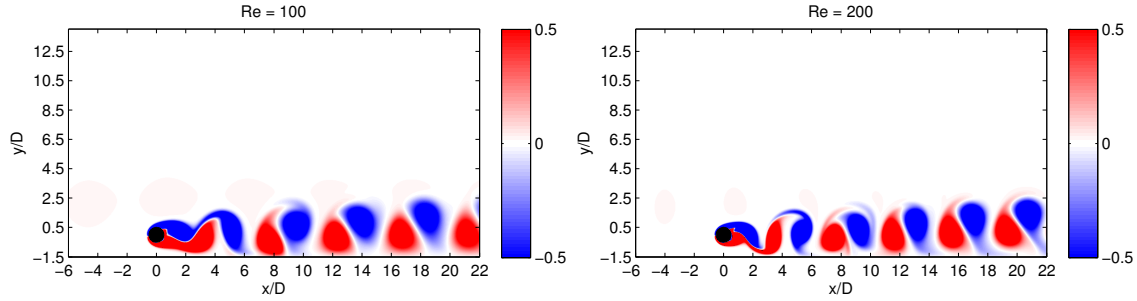

(a) Single cylinder.

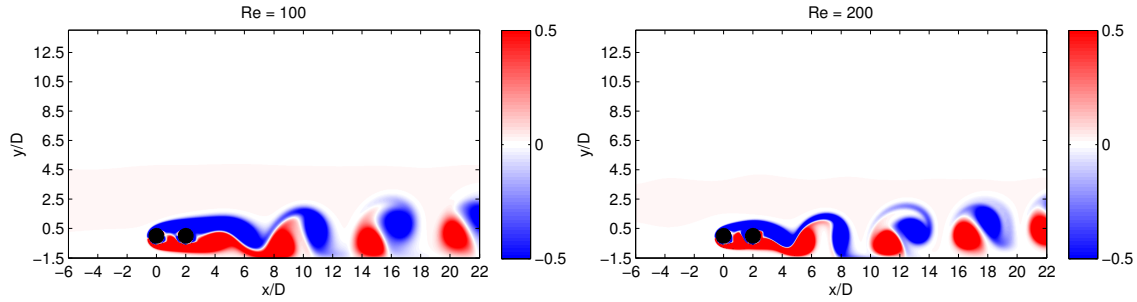

(b) Two tandem cylinders with $^{L}/_{D} = 2$.

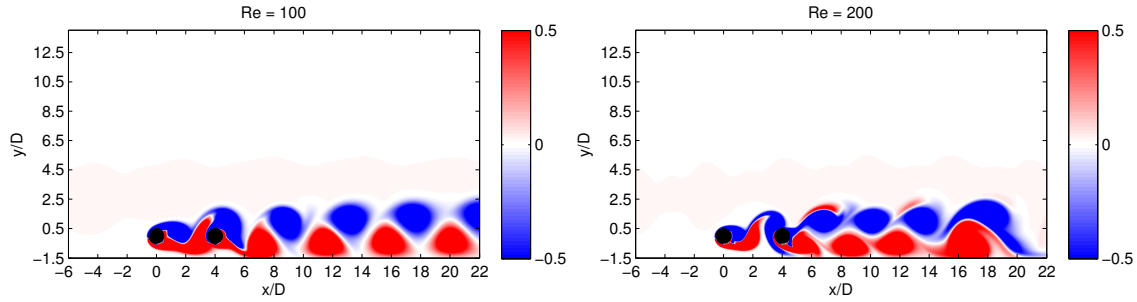

(c) Two tandem cylinders with $^{L}/_{D} = 4$.

Figure 5.2: Vorticity contours for $^{G}/_{D} = 1$

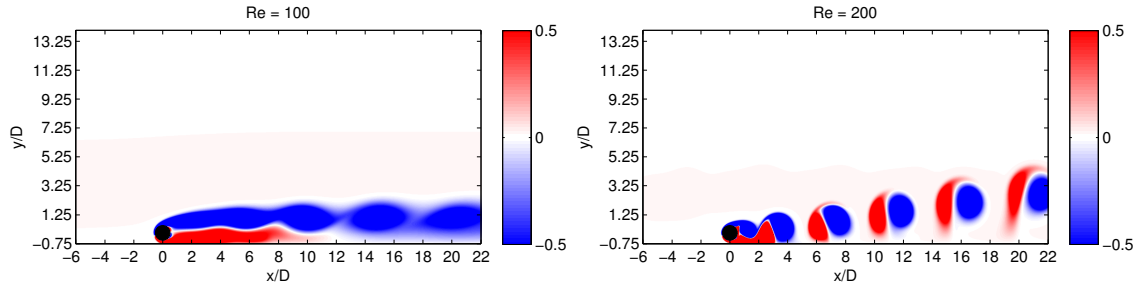

(a) Single cylinder.

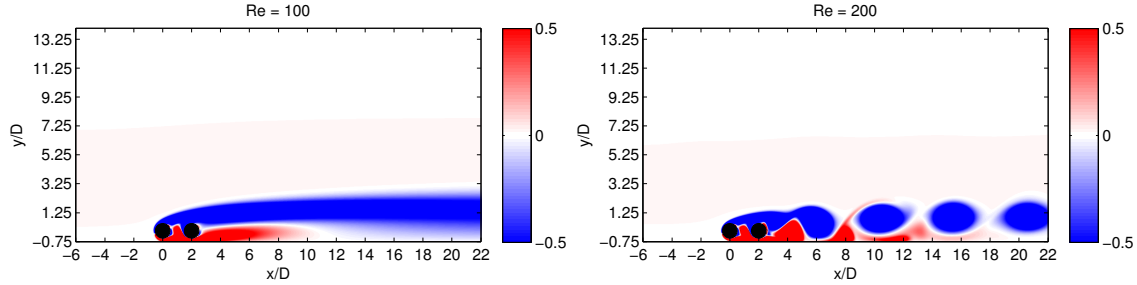

(b) Two tandem cylinders with $L/D = 2$.

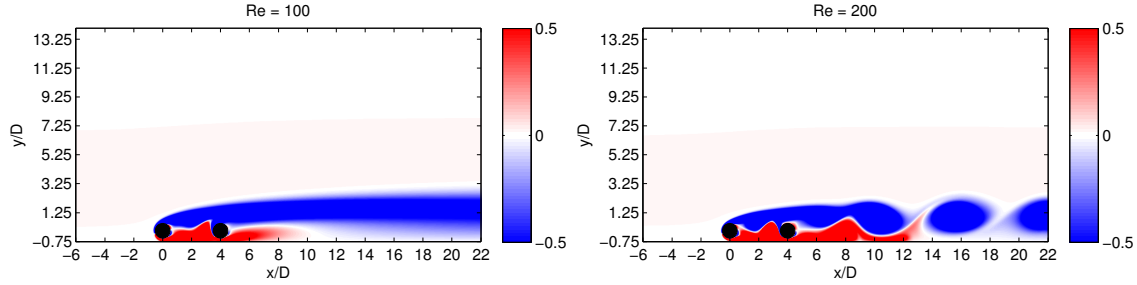

(c) Two tandem cylinders with $L/D = 4$.

Figure 5.3: Vorticity contours for $G/D = 0.25$

5.2.1 Variation of Strouhal number with gap ratio

The Strouhal number St is a non-dimensional parameter that describes the oscillatory motion of a fluid configuration. For fixed cylinders:

$$St = \frac{f \cdot L_c}{U_c} \tag{5.1}$$

, where f is the frequency of vortex shedding. In this problem $L_c = D$ and $U_c = U_\infty$.

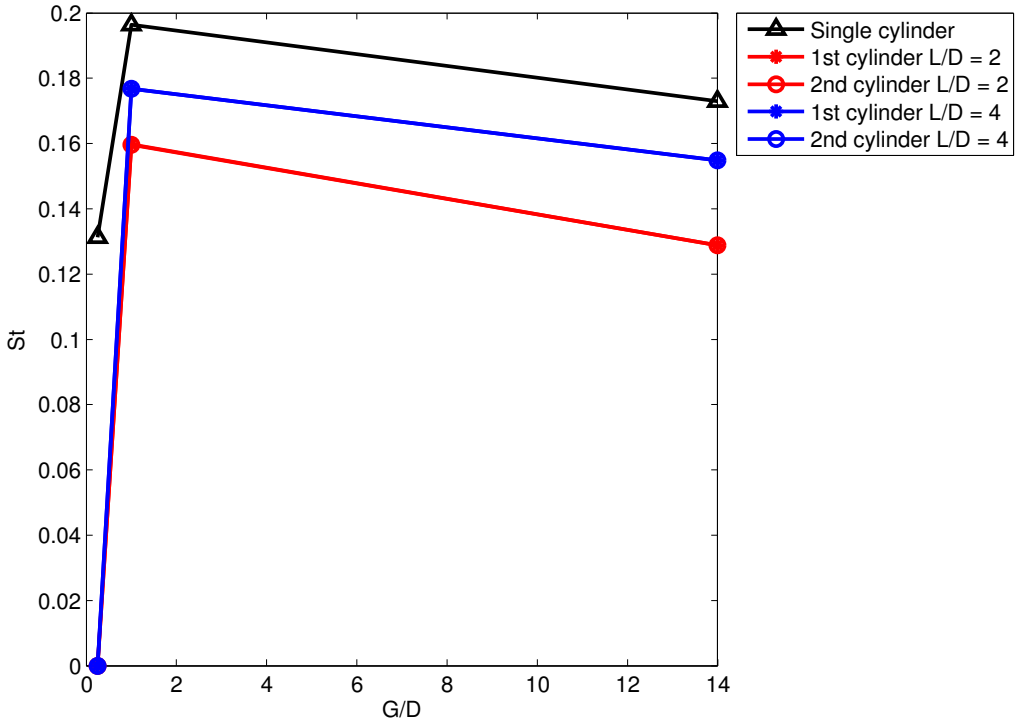

(a) Re=100

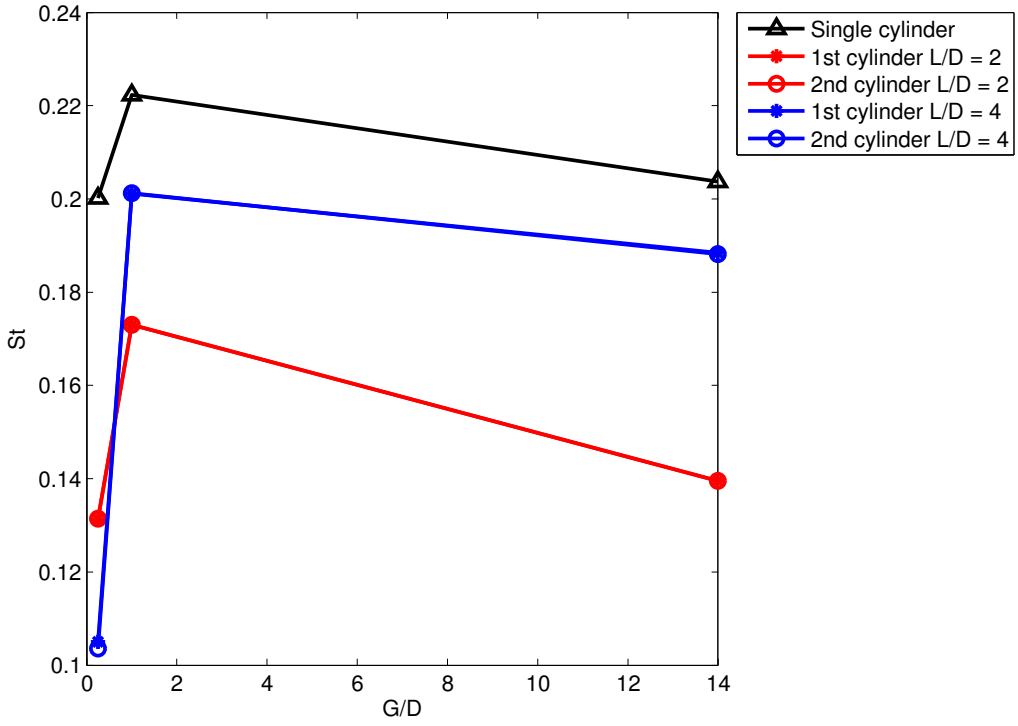

(b) Re=200

Figure 5.4: Strouhal number versus gap for cases with $Re = 100$ (a) and $Re = 200$ (b).

Figure 5.4 shows the comparison between the Strouhal number and the gap ratio for different $^{L}/_{D}$ configurations. *Figures 5.4a* and *5.4b* are for $Re = 100$ and $Re = 200$, respectively.

The legend indicates 5 types of curves corresponding to three different test cases. However, only three curves are distinguished in the graph because the Strouhal number for the 1^{st} and 2^{nd} cylinder is coincident.

It can be observed that for both Reynolds number, the single cylinder configuration has a higher Strouhal number than the pair of cylinders. At higher Re, the St is also higher for every configuration, so the vortex shedding is more frequent. This increase in shedding frequency with Re is more evident in the representation of the vorticity in *figures 5.1, 5.2* and *5.3*.

Note that for the pair of cylinders at $Re = 100$ closest to the wall ($^G/_D = 0.25$), vortex shedding is not triggered. This happens for the single cylinder configuration as well, but the vorticity contour in *figure 5.3a* shows an attempt at transitioning to vortex shedding. This could be caused by the confinement effect combined with low enough Reynolds numbers.

At $Re = 200$, the single cylinder develops vortex shedding from the upper and lower part of the cylinder, whereas for the pair of cylinders, the vortices develop only from the upper part. At this Reynolds number, the increase in gap ratio from $^G/_D = 0.25$ to $^G/_D = 1$ has a greater impact on the increase of the Strouhal number for $^L/_D = 4$ as compared with $^L/_D = 2$. Vortex shedding at $^G/_D = 0.25$ occurs at a higher Strouhal number for $^L/_D = 2$. On the other hand, at $^G/_D = 1$, the Strouhal number is greater for $^L/_D = 4$.

5.2.2 Variation of aerodynamic forces with gap ratio and Reynolds

Single cylinder

The fluctuation of the aerodynamic forces of a single cylinder when approaching the free-slip wall is depicted in *figures 5.5* and *5.6*.

The mean value of the lift coefficient increases as the gap ratio becomes smaller for both Reynolds number. For $Re = 100$, the amplitude of the lift coefficient increases from isolated to $^G/_D = 1$ but decreases to almost 0 for the closest gap ratio, where the vortex shedding is suppressed. For $Re = 200$, the amplitude does not follow the same behavior as $Re = 100$. In this case, the amplitude of the oscillations increases in spite of the confinement effect.

The mean value of the drag coefficient tends to increase as the cylinder gets closer to the wall, unless vortex shedding is not triggered. When there is no vortex shedding in the wake, the mean value of the drag is smaller for $^G/_D = 0.25$ than $^G/_D = 1$. This occurs at $Re = 100$. A similar tendency is observed for the amplitude of the drag coefficient.

For the isolated cylinder/s, the problem is symmetric in the x direction. For a full period of the lift, two periods of the drag have been completed, and $St_D = 2St_L$, where St_D and $St_L$are the Strouhal numbers for the drag and lift, respectively. When approaching a wall, the problem becomes asymmetric and the periodic behavior of the drag changes, as observed for the case of $^G/_D = 1$ at either Reynolds number. In a single period there are two oscillations. The first oscillation is bigger in amplitude than the second. The two oscillations within one period are the result of irregular strength in vortex shedding process. The vortex in the upper part is stronger than the vortex in the lower part, causing this peculiarity in the fluctuation of the drag coefficient, whose period is now similar to the period of the lift (more clearly seen for $^G/_D = 0.25$).

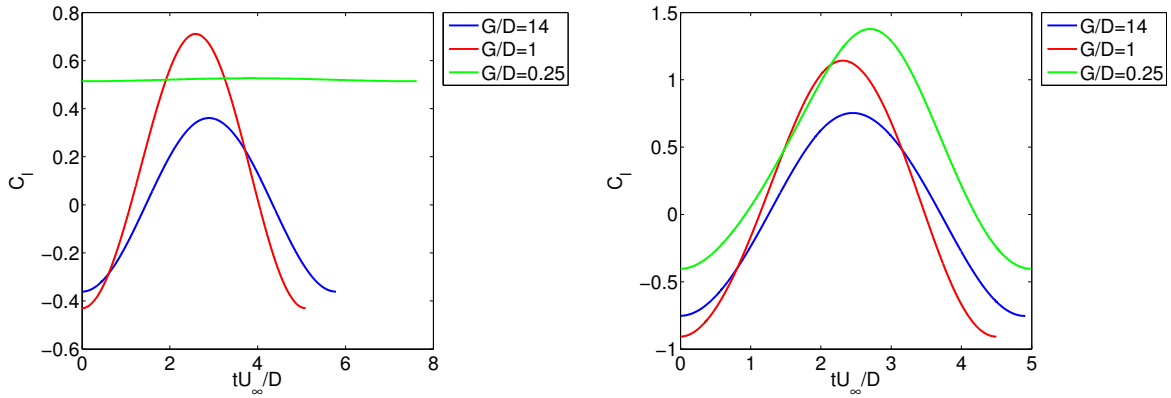

(a) $Re = 100$ (b) $Re = 200$

Figure 5.5: Single cylinder. Lift coefficient versus non-dimensional time. Single period.

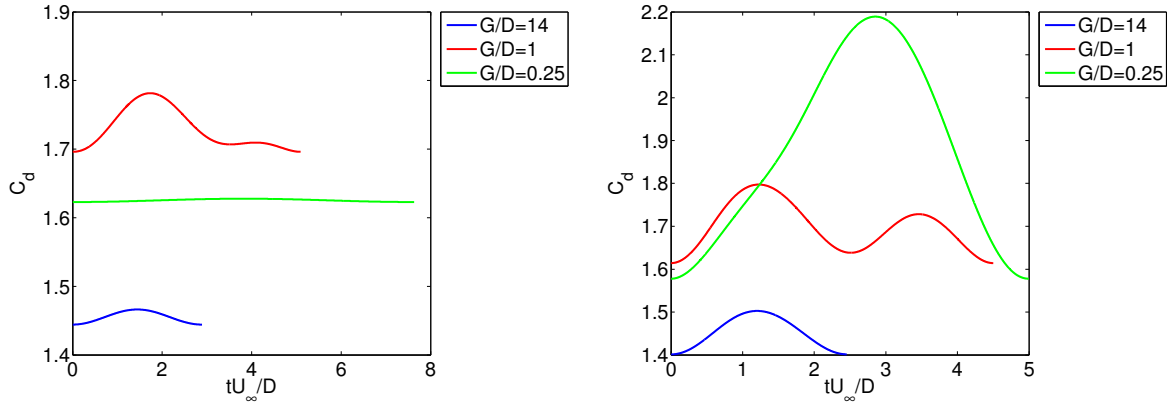

(a) $Re = 100$ (b) $Re = 200$

Figure 5.6: Single cylinder. Drag coefficient versus non-dimensional time. Single period.

Two cylinders in tandem with $^{L}/_{D} = 2$

The fluctuations in the forces of two tandem cylinders approaching the free-slip wall are more complex than those of the single cylinder, because the two cylinders behave as one extended-body for $^{L}/_{D} = 2$. The aerodynamic forces are represented in *figures 5.7* and *5.8*.

The mean value of the lift coefficient increases for both cylinders and Reynolds number when approaching the wall. At $Re = 100$, for the isolated case and $^{G}/_{D} = 1$ the amplitude is small for the first cylinder, but more significant for the second, since vortex shedding occurs only in the wake of the second cylinder (extended-body regime). For the gap ratio $^{G}/_{D} = 0.25$, there is no vortex shedding, hence no amplitude in the lift coefficient.

The drag coefficient has an interesting behavior for the case of longitudinal separation between the cylinders of $^{L}/_{D} = 2$. As was mentioned above, the two cylinders behave as a single bluff body. The consequence is the complete suppression of vortex shedding from the first cylinder. The shedding is delayed and happens further downstream from

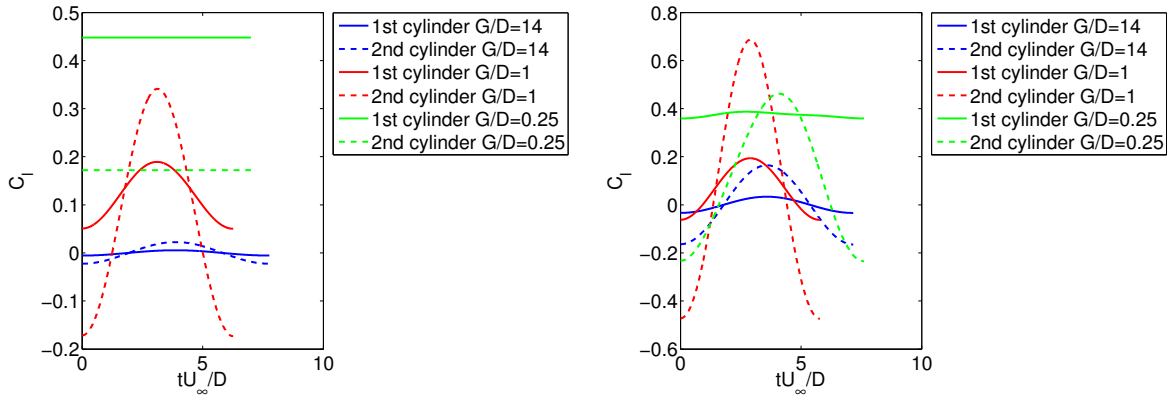

(a) $Re = 100$ (b) $Re = 200$

Figure 5.7: Tandem cylinder with $^{L}/_{D} = 2$. Lift coefficient versus non-dimensional time. Single period.

the end of the second cylinder than it does for the case of a single cylinder. This is reflected in the behavior of the drag coefficient, where the amplitude is small, almost non-existent. Moreover, for the isolated configuration, the second cylinder experiences thrust instead of drag. The lack of confinement effect and the proximity to the first cylinder, shielding the second from the incoming flow, produces this effect.

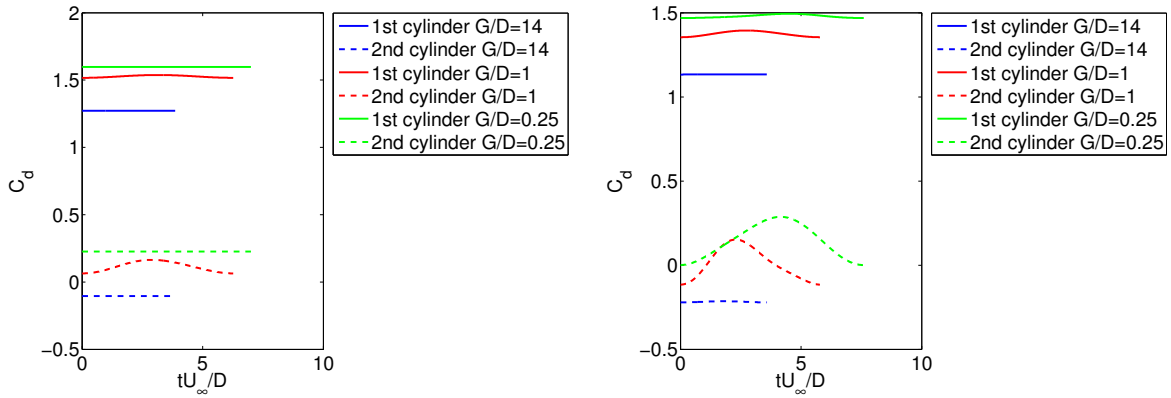

(a) $Re = 100$ (b) $Re = 200$

Figure 5.8: Tandem cylinder with $^{L}/_{D} = 2$. Drag coefficient versus non-dimensional time. Single period

Two cylinders in tandem with $^{L}/_{D} = 4$

The flow patterns of the two cylinders in tandem with $^{L}/_{D} = 4$ correspond to the shear-layer reattachment regime, except for the case of $Re = 100$ and $^{G}/_{D} = 0.25$, where the cylinders behave as an extended body. The aerodynamic forces for this configuration are represented in *figures 5.9* and *5.10*.

The tendency of the mean value of the lift is to increase with smaller gap ratios for both Reynolds numbers. The difference in mean lift coefficient between $^{G}/_{D} = 0.25$ and

$G/D = 1$ is not evident. There is no amplitude of the lift coefficient for the gap ratio $G/D = 0.25$ because there is no vortex shedding ($Re = 100$) or the vortex shedding is from the upper part of second cylinder far enough downstream not to affect the body. For the gap ratio $G/D = 1$ and the isolated configuration at $Re = 200$, the behavior in amplitude of the first cylinder of the isolated configuration is very similar to the first cylinder of $G/D = 1$. The same happens with the second cylinder.

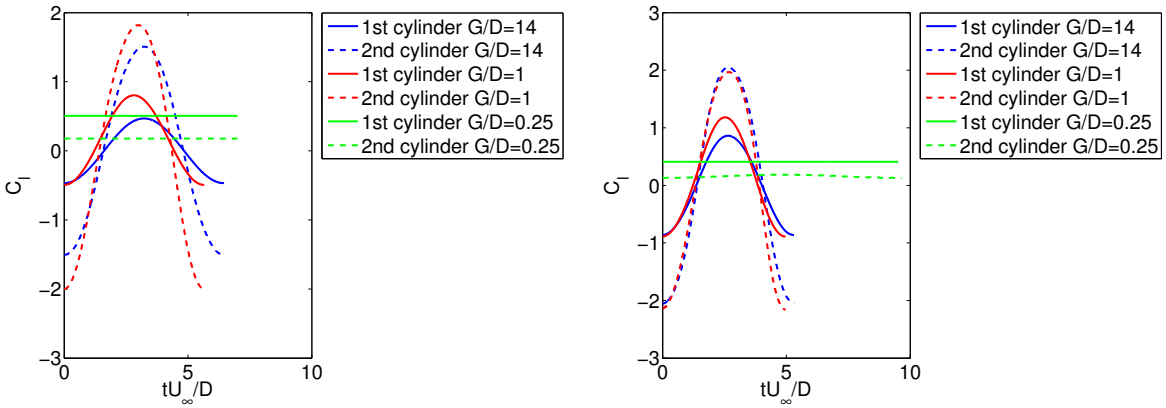

(a) $Re = 100$ (b) $Re = 200$

Figure 5.9: Tandem cylinder with $L/D = 4$. Lift coefficient versus non-dimensional time. Single period.

For $Re = 100$ and $Re = 200$, the mean value of the drag coefficient increases with smaller gap ratios except for $G/D = 0.25$ because there is no vortex shedding ($Re = 100$), or the vortex shedding is weak and only shed from the upper part of the cylinder far enough downstream. For $G/D = 1$, appears again the two oscillations within one period as a result from strength irregularities in the vortex shedding, where the upper vortices are stronger than the lower vortices.

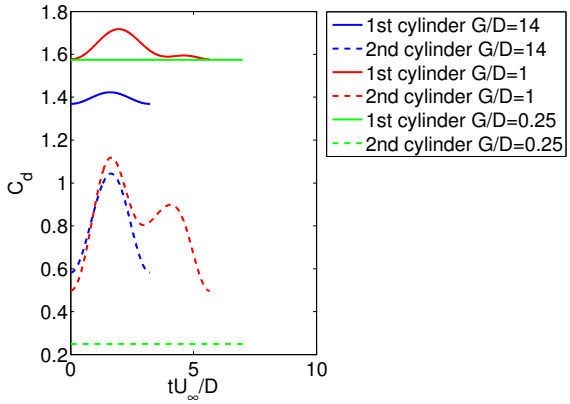

(a) $Re = 100$

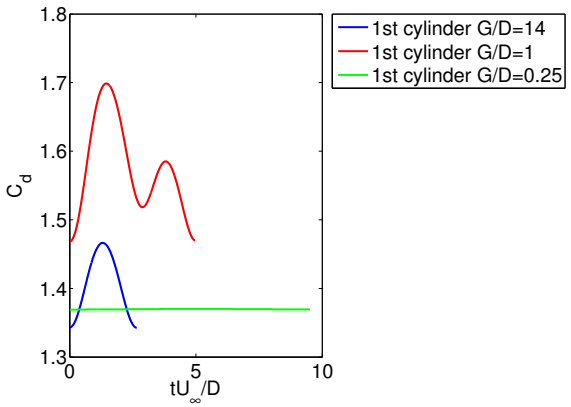

(b) $Re = 200.\ 1^{st} cylinder$

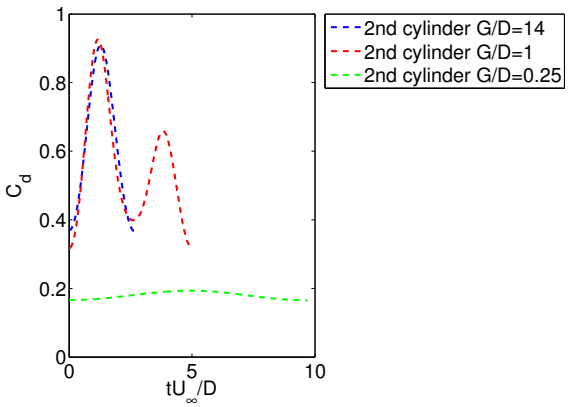

(c) $Re = 200.\ 2^{nd} cylinder$

Figure 5.10: Tandem cylinder with $^{L}/_{D} = 4$. Drag coefficient versus non-dimensional time. Single period.

Chapter 6

Conclusions

This project has made use of a Direct Numerical Simulation to solve the fluid dynamic problem of flow past circular cylinders in tandem in the proximity of a plane wall. The key parameters, responsible for the aerodynamic forces fluctuations and the variations in vortex shedding frequency (Strouhal number), have been combined to produce different problem configurations to achieve a better understanding of the interactions between bodies and the proximity to a free-slip wall.

The evaluation of the Strouhal number shows that the single cylinder configuration has a higher shedding frequency than the tandem configuration. In addition, the Strouhal number increases with increasing Reynolds numbers.

The complex flow patterns developed with the proximity to a plane wall have also been analyzed. For instance, with a constant longitudinal separation ($^{L}/_{D} = 4$), the flow pattern changes as the cylinders get closer to the wall from shear-layer reattachment to extended body regime. This shows that there is a critical point of the separation to the wall that achieves vortex shedding suppression for the first and/or the second cylinder, as a function of the Reynolds. Thus, the confinement effect and the low Reynolds number are the key parameters in this particular phenomena.

The proximity to the wall affects the mean value of the forces, as they increase the closer the bodies are with respect to the wall. The fluctuations on the aerodynamic forces are produced by the shedding of vortices. The distance from the body to the beginning of the vortex shedding is related to the amplitude. The closer to the body, the higher the amplitude.

6.1 Future work

Regarding future work, the first action to continue the research in this project could be to enlarge the set of values for the evaluated parameters (Re, $^{L}/_{D}$, $^{G}/_{D}$ and number of cylinders). This would allow for a more accurate analysis of the behavior, the tendencies and critical points there may be in between the studied configurations.

Moreover, the project has been focused on isolating the effect of confinement from the effect of no-slip of an actual solid wall. The work developed could be complemented with two more steps to better understand the interaction of a body with a plane wall. On one hand, isolating the velocity gradient, as was done for the confinement effect. On the other hand, simulating an actual solid wall (or a model as close to reality as possible).

With the data from these three types of simulations, a complete analysis could be made to assess which parameters are responsible for the effects on the problem configuration.

In addition, a step further into this line of research could be to analyze the test cases posed in this project with cylinders that are free to vibrate as a result of the fluctuating forces acting on the body, as well as the interaction with other bodies and the proximity to a plane wall. This application is called vortex induced vibrations (VIV).

Appendix A

Budget

To consider this project complete, an estimation of the costs derived from its development is simulated.

Nevertheless, most of the costs detailed below are University resources already provided as part of the research material for the University community. The actual costs of said resources are not readily available. In those cases, other sources have been used as a reference to simulate the total cost of a project such as this one.

Item	Description & usage	Quantity	Cost	Price
Laptop	Model: Acer Aspire 3820TG-334G50N. Necessary tool for pre- and post-processing data from the simulations	1	799 €/unit	799 €
Cluster usage	Every run simulation uses a certain computational space that is generally paid by the hour and number of nodes.	200 core-hour	0.011186 €/core-hour	2.2372 €
MATLAB ®	Matlab individual license for post processing the data extracted from the simulations	1	2000 €/unit	2000 €
CFD Software	One year license for a fluid solver such as Fluent	1	6000 €/unit	6000 €
Engineering work		500 h	42 €/h	21,000 €
TOTAL				29,801.2372 €

Table A.1: Project cost estimation

Bibliography

[1] http://www.elarasystems.com/industrialstills3.html.

[2] Christoffer Norberg. Fluctuating lift on a circular cylinder: review and new measurements. *Journal of Fluids and Structures*, 17(1):57–96, 2003.

[3] http://www.atmos.washington.edu/2010q1/536/figs/lee%20vortex/nafrica_2_01.2005005.aqua.250m-c.jpg.

[4] D Sumner. Two circular cylinders in cross-flow: a review. *Journal of Fluids and Structures*, 26(6):849–899, 2010.

[5] Charles Hirsch. Chapter 2 - the dynamical levels of approximation. In Charles Hirsch, editor, *Numerical Computation of Internal and External Flows (Second Edition)*, pages 65 – XIII. Butterworth-Heinemann, Oxford, second edition edition, 2007.

[6] MM Zdravkovich. The effects of interference between circular cylinders in cross flow. *Journal of Fluids and Structures*, 1(2):239–261, 1987.

[7] Seikan ISHIGAI, Eiichi NISHIKAWA, Keiya NISHIMURA, and Katsuzo CHO. Experimental study on structure of gas flow in tube banks with tube axes normal to flow: Part 1, karman vortex flow from two tubes at various spacings. *Bulletin of JSME*, 15(86):949–956, 1972.

[8] MM Zdravkovich. Flow induced oscillations of two interfering circular cylinders. *Journal of Sound and Vibration*, 101(4):511–521, 1985.

[9] AA Hetz, MN Dhaubhadel, and DP Telionis. Vortex shedding over five in-line cylinders cylinders. *Journal of Fluids and Structures*, 5(3):243–257, 1991.

[10] http://oceanservice.noaa.gov/facts/eddy.html.

[11] G Xu and Y Zhou. Strouhal numbers in the wake of two inline cylinders. *Experiments in Fluids*, 37(2):248–256, 2004.

[12] Y Zhou and MW Yiu. Flow structure, momentum and heat transport in a two-tandem-cylinder wake. *Journal of Fluid Mechanics*, 548:17–48, 2006.

[13] Tamotsu Igarashi. Characteristics of the flow around two circular cylinders arranged in tandem. i. *JSME International Journal Series B*, 24:323–331, 1981.

[14] http://www.dosits.org/tutorials/sciencetutorial/speed/.

[15] http://oceanmotion.org/html/background/wind-driven-surface.htm.

[16] http://www.grc.nasa.gov/www/k-12/airplane/nseqs.html.

[17] David L Brown, Ricardo Cortez, and Michael L Minion. Accurate projection methods for the incompressible navier–stokes equations. *Journal of Computational Physics*, 168(2):464–499, 2001.

[18] Joel H Ferziger and Milovan Perić. *Computational methods for fluid dynamics*, volume 3. Springer Berlin, 2002.

[19] Richard Courant, Kurt Friedrichs, and Hans Lewy. Über die partiellen differenzengleichungen der mathematischen physik. *Mathematische Annalen*, 100(1):32–74, 1928.

[20] Markus Uhlmann. An immersed boundary method with direct forcing for the simulation of particulate flows. *Journal of Computational Physics*, 209(2):448–476, 2005.

[21] http://www.techterms.com/definition/cluster.

[22] Unitsa Sangket, Surakameth Mahasirimongkol, Wasun Chantratita, Pichaya Tandayya, and Yurii S Aulchenko. Parallabel: an r library for generalized parallelization of genome-wide association studies. *BMC bioinformatics*, 11(1):217, 2010.

[23] AB Harichandan and A Roy. Numerical investigation of flow past single and tandem cylindrical bodies in the vicinity of a plane wall. *Journal of Fluids and Structures*, 33:19–43, 2012.

[24] Ignacio Verona Ríos. Instalación y configuración de un cluster de alto rendimiento. pages 83–84, 2010.

[25] Susana Izquierdo Bermúdez. Towards the numerical simulation of the filling process of the left ventricle of the heart. 2010.

[26] RD Gabbai and H Benaroya. An overview of modeling and experiments of vortex-induced vibration of circular cylinders. *Journal of Sound and Vibration*, 282(3):575–616, 2005.

[27] E Guilmineau and P Queutey. A numerical simulation of vortex shedding from an oscillating circular cylinder. *Journal of Fluids and Structures*, 16(6):773–794, 2002.

[28] Frank M White. Fluid mechanics, wcb, 1999.

[29] http://www.mathworks.es/pricing-licensing/index.html?prodcode=ml&s_iid=main_pl_ml_tb, 2014.

[30] http://www.notebookcheck.org/acer-aspire-3820tg-334g50n.30372.0.html.

[31] http://idi.ucsd.edu/computing/#tscc-costs.